Available online at www.sciencedirect.com

ScienceDirect

Underground Space 27 (2026) 175–193

www.keaipublishing.com/undsp

Research Paper

Seismic damage characteristics and resilience design of cross-fault tunnels: New insights from the Daliang Tunnel in the 2022 Menyuan M_W6.6 Earthquake

Haitao Yu [a,b,*], Yibo Wei [a], Yong Yuan [a,b], Guoliang Li [c], Hehua Zhu [a,b]

[a] *Department of Geotechnical Engineering, College of Civil Engineering, Tongji University, Shanghai 200092, China*
[b] *State Key Laboratory of Disaster Reduction in Civil Engineering, Tongji University, Shanghai 200092, China*
[c] *China Railway First Survey and Design Institute Group CO., LTD., Xi'an 710000, China*

Received 3 December 2024; received in revised form 3 February 2025; accepted 5 March 2025
Available online 5 January 2026

Abstract

An earthquake with a magnitude of 6.6 (M_W) occurred in Menyuan County, Qinghai Province, China, on January 8th, 2022. The Daliang Tunnel, which traverses the seismogenic fault, was severely damaged during this seismic event. The seismic damage investigation of the tunnel is introduced, and the damage characteristics along the tunnel are also presented. It is found that the damage severity of the tunnel is highly correlated with the distance to the fault. Damage modes for different tunnel zones (cross-fault zone, portal zone, and ordinary zone far from the fault and the portal) are quite distinct. Based on the understanding of seismic damage to the Daliang Tunnel in 2022 Menyuan Earthquake, as well as other damaged tunnels during the 2008 Wenchuan Earthquake, the critical influence factors for damage to cross-fault tunnels are discussed. From the seismic investigation, coupling effects of strong ground motions and fault dislocations are highlighted, which pose significant risks to cross-fault tunnels and should be considered in the seismic design for such tunnels. The deformation joints of the tunnel could help the tunnel adapt to the deformation caused by fault dislocation, and thus protect the main structure, but inversely an added local deformation may be expected around the deformation joints. The instability of the overlying slope may have contributed to the local amplification of the fault dislocation along the Daliang Tunnel. Finally, the requirements of seismic resilience for cross-fault tunnels are proposed, and detailed suggestions are provided to enhance the seismic performance of such cross-fault tunnels.

Keywords: Earthquake; Damage investigation; Cross-fault tunnel; Deformation joint; Dislocation spatial variability; Seismic resilience

1 Introduction

Tunnels, as crucial components of lifeline engineering, are expected to remain operational after earthquakes to facilitate post-earthquake rescue and relief efforts. Historical cases of seismic damage investigation indicate that tunnels crossing faults are particularly vulnerable during earthquakes (Asakura, 1997; Wang et al., 2001; Yu et al., 2016b). The seismic performance of such tunnels has been the focus of research for decades. Despite these efforts, the significant damage observed at the Daliang Tunnel during the 2022 Menyuan Earthquake (M_W6.6) highlights ongoing challenges in ensuring the safety of cross-fault tunnels in seismically active regions. This incident further emphasizes the need for improved design strategies for tunnels in seismic zones.

Field investigation after an earthquake is always an efficient way to intuitively study the seismic behavior of tunnels and thus has become an essential work after earthquakes. Asakura and Sato (1996) assessed over 100 tunnels in the seismic zone of the 1995 Hyogoken-Nanbu Earth-

* Corresponding author at: Department of Geotechnical Engineering, College of Civil Engineering, Tongji University, Shanghai 200092, China.
E-mail address: yuhaitao@tongji.edu.cn (H. Yu).
Peer review under the responsibility of Tongji University

https://doi.org/10.1016/j.undsp.2025.03.009

quake, and found that around ten tunnels required extensive renovation, especially for the Rokko Tunnel that passed through faults. Wang et al. (2001) established a database of 57 tunnels affected by the 1999 Chi-Chi Earthquake, recording that at least two cross-fault tunnels suffered severe damage. After the 2008 Wenchuan Earthquake, a number of researchers investigated and assessed all the damaged highway tunnels, and five of them crossed active faults (Chen, 2012; Shen et al., 2014; Wang et al., 2009; Wang & Zhang, 2013; Yu et al., 2016a). Zhang et al. (2018, 2019) investigated the seismic damage to the Tawarayama Tunnel in the 2016 Kumamoto Earthquake and analyzed the correlation between seismic damage of the tunnel and ground deformation induced by the Futagawa Fault. Zhang et al. (2020) compiled a database of tunnel damage caused by faults in 12 historical earthquakes. Note that the focus of these studies is to establish a comprehensive seismic damage database for tunnels and analyze the potential factors affecting tunnel damage during earthquakes. Recently, seismic damage to tunnels crossing faults is still continuously reported, such as the Daliang Tunnel affected by the 2022 Menyuan Earthquake, while sections close to the fault have completely collapsed. The damage provides sufficient evidence to suggest that the safety of tunnels in seismic active zones is still an important issue and should be taken as a warning for the need for better design of tunnels in seismically active areas.

The conventional seismic design strategies for tunnels crossing active faults primarily focus on ensuring that the tunnel structure can accommodate predicted fault displacements while allowing for post-earthquake lining repairs (Shen et al., 2020), which highlight the need for the implementation of appropriate seismic fortification and control measures. Current seismic mitigation strategies for tunnels crossing active faults mainly involve the enhancement or optimization of either the tunnel structure itself or the surrounding rock mass properties (Ansari et al., 2024; Zhao et al., 2022). However, existing seismic prevention and control measures for tunnels crossing active faults have not adequately incorporated the seismic resilience objectives of the engineering system, and accordingly, it is essential to develop new mitigation strategies that specifically address post-earthquake tunnel rehabilitation, resilience enhancement, and rapid restoration of traffic capacity. Furthermore, a unified design concept for seismic resilience in tunnels crossing active faults is still missing, which is, however, very important for guiding the entire process of seismic resilience design.

This paper presents in detail the seismic damage observed at the Daliang Tunnel during the 2022 Menyuan M_W6.6 Earthquake, and the tunnel section crossing an active seismogenic fault was adversely affected by the earthquake. The distribution of damage patterns along the tunnel is described, and the tunnel damage zones are also classified. The critical factors affecting seismic damage of such cross-fault tunnels are discussed and summarized, based on the understanding of seismic damage to the Daliang Tunnel in the 2022 Menyuan Earthquake, as well as other damaged tunnels in the 2008 Wenchuan Earthquake. Note that the two earthquakes both occurred in western China. Furthermore, seismic resilience requirements for cross-fault tunnels are discussed, and concrete suggestions are also provided to improve the seismic performance of such cross-fault tunnels.

2 Overview of the 2022 Menyuan Earthquake and the Daliang Tunnel

2.1 2022 Menyuan M_W6.6 Earthquake

On January 8, 2022, at 1:45 a.m. local time, a strong earthquake with a moment magnitude of 6.6 struck Qinghai Province in China. The epicenter, with a focal depth of 10 km, is located in Menyuan County at a latitude of 37.77°N and a longitude of 101.26°E. This seismic event was triggered by the dislocation of the Lenglongling Fault (LLL Fault), which was situated in the central and western segment of the Qilian-Haiyuan Fault along the northern margin of the Qinghai-Tibet Plateau. The spatial relationship between the epicenter, the main ground surface rupture, and the Daliang Tunnel is illustrated in Fig. 1. The epicenter is approximately 3–4 km south of the main ground surface rupture of the LLL Fault and about 4.5 km west of the Daliang Tunnel. The intersection between the Daliang Tunnel and the LLL Fault is about 500 m from the northern portal of the tunnel, with a cross angle of around 50°.

2.2 Lenglongling fault

The LLL Fault is the seismogenic fault of this seismic event, generating a main surface rupture of 21.5 km with a nearly east–west strike. It is characterized as both a left-lateral strike-slip and thrust fault, with maximum horizontal and vertical dislocation reaching 3.1 and 0.9 m, respectively. The local horizontal dislocation of this surface rupture at the slope overlying the Daliang Tunnel is about 2.77 m (Liang et al., 2022), as depicted in Fig. 2. Additionally, the dip angle of the LLL Fault is about 70°, and its width is 295 m, from K1971+385 to K1971+680, as shown in Fig. 3(b).

Figure 3(a) displays the longitudinal vertical section of the tunnel site, including geological conditions along the tunnel and geometric features of the LLL Fault. The Daliang Tunnel is a double-track railway tunnel with a maximum buried depth of 800 m. The stratum lithology of the tunnel site mainly consists of the Middle Ordovician slate, sandstone, limestone, and Permian sandstone. Quaternary silty soil, fine breccia soil, coarse breccia soil, gravel soil, and rocky soil are distributed in the slope and gully. Cataclasite-type fault rock is presented in the fault fracture zone.

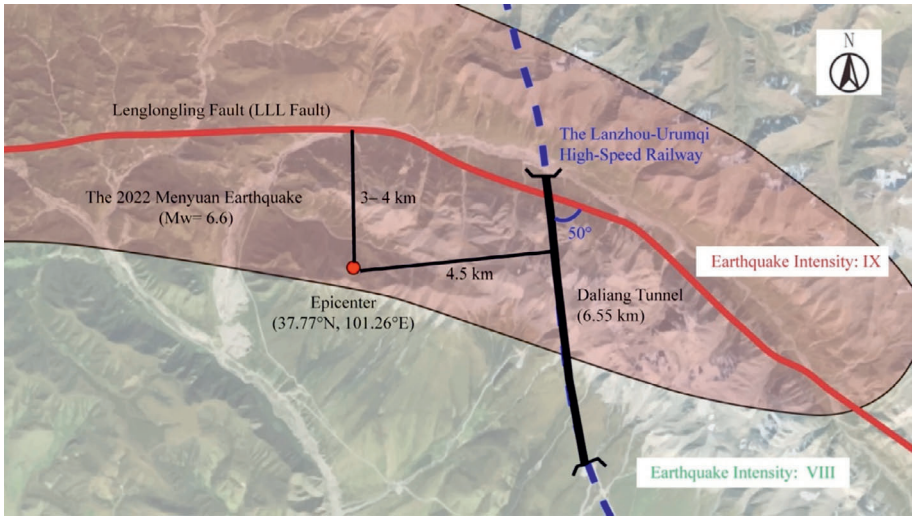

Fig. 1. Location of the Daliang Tunnel and the epicenter of the 2022 Menyuan Earthquake. (Data from China Earthquake Administration (2022)).

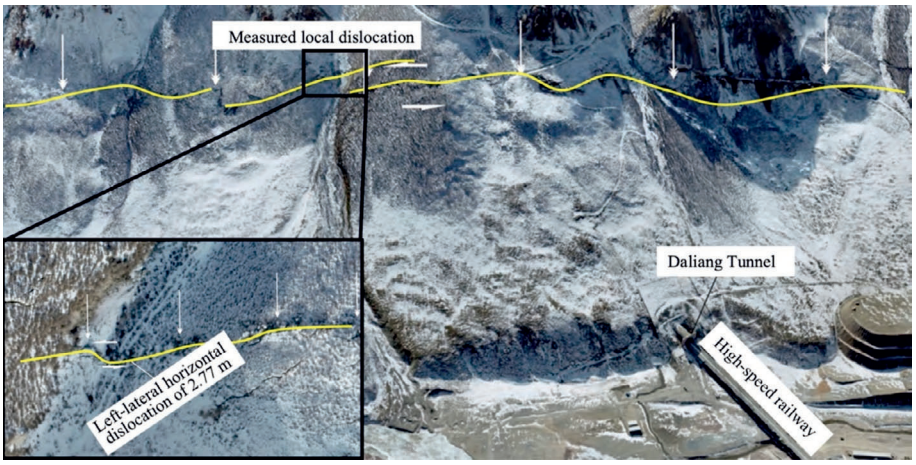

Fig. 2. Faulted landform of the Daliang Tunnel site (Liang et al., 2022).

The surrounding rocks along the tunnel are organized into three classes according to the Code for Design of Railway Tunnel (China Railway Eryuan Engineering Group Co., Ltd., 2016), namely grade III, IV, and V. The properties of the surrounding rocks are worse with growing grade numbers. The classification and corresponding mileages of the surrounding rocks are annotated in Fig. 3. It can be seen that the rock class of over 70% zone in the tunnel site is grade V, including the LLL Fault, indicating that the surrounding rock properties in the tunnel site are relatively poor.

2.3 Daliang tunnel

The Daliang Tunnel has a total length of 6.55 km and traverses two different earthquake intensity regions. The tunnel segment, extending 4670 m from the northern portal to the inner section, is located in the earthquake intensity region with IX degree, while the remainder is situated in the region of VIII degree earthquake intensity, as illustrated in Fig. 1 according to the Earthquake Intensity Map of the Menyuan M_S6.9 Earthquake (China Earthquake Administration, 2022).

Deformation joints are installed along the tunnel at intervals of 10 m, dividing it into segments. The typical cross-section of the Daliang Tunnel is a horseshoe-shaped section, as shown in Fig. 4, with a width of 15.40 m and a height of 12.88 m. The tunnel support system consists of primary support, molded support, a waterproof layer, and secondary lining. The primary support is composed of 0.3 m-thick shotcrete, steel arches, and rock bolts with a spacing of 1 m and a length of 4 m. The molded support consists of 0.3 m thick molded concrete and steel grilles, while the secondary lining is made of 0.4 m thick reinforced concrete. The concrete used for the tunnel system is C25-grade for the primary support and C30-grade for the molded support and secondary lining (the grade is consistent with the Code for Design of Concrete Structures

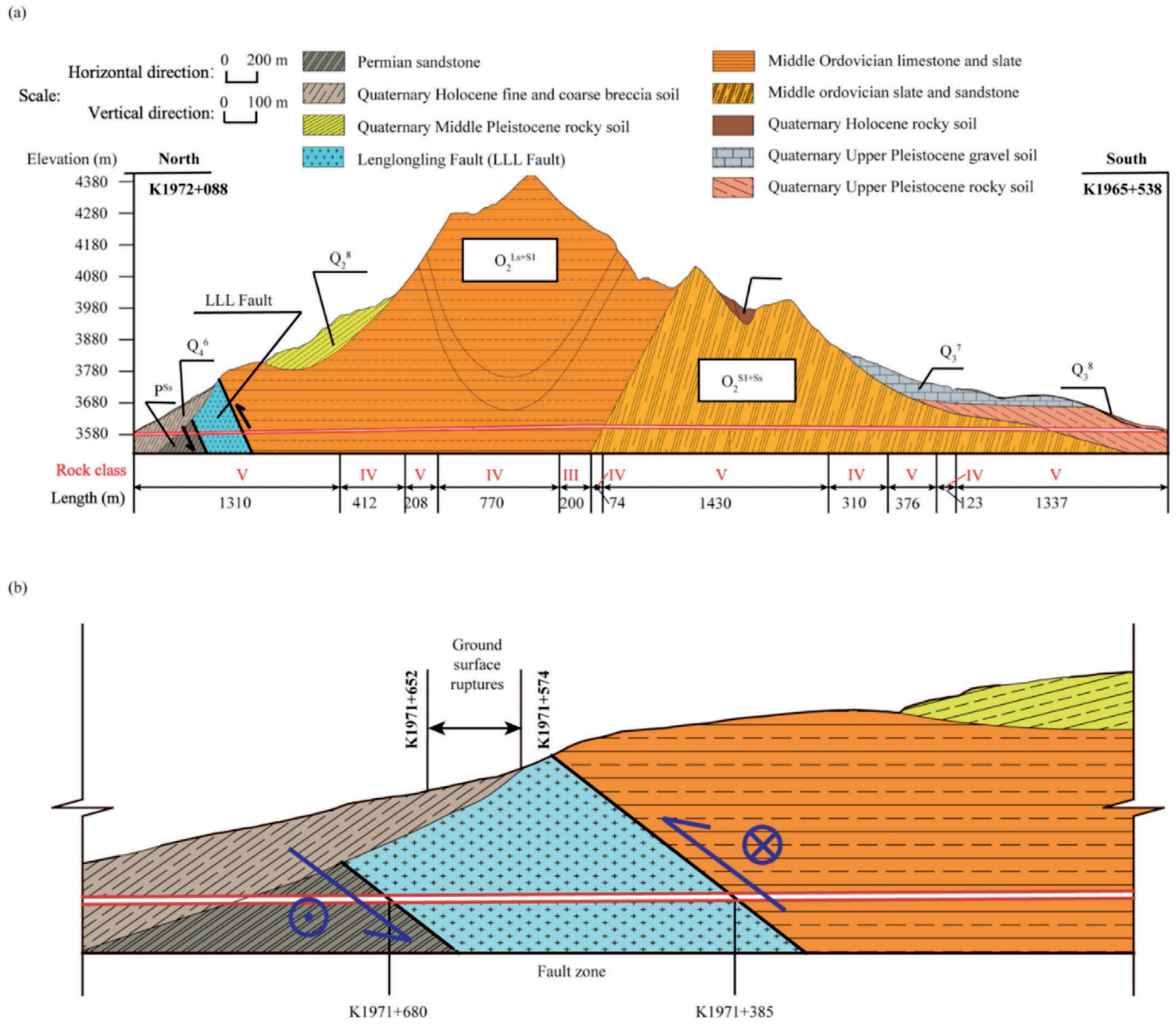

Fig. 3. Longitudinal profile of the Daliang Tunnel site. (a) Overview of the surrounding rock properties and local geography, and (b) geometry of the LLL Fault.

(Ministry of Housing and Urban-Rural Development of the People's Republic of China, 2010).

3 Seismic damage characteristics of the Daliang Tunnel

3.1 Damage classification

3.1.1 Dislocation of tunnel lining

The most significant damage to the Daliang Tunnel occurred in the form of lining dislocation, concentrated within a 350 m range in the vicinity of the LLL Fault, from K1971+341 to K1971+691. Notably, 295 m of this range were entirely located within the fault zone, while 44 m were situated in the hanging wall and 11 m in the footwall.

Figure 5 shows the most severely damaged part of the tunnel across the fault, where it is clearly visible that the left hence of the tunnel lining completely collapsed, with the secondary lining of the left sidewall squeezed inward by approximately 1.5 m. The deformation joint of the right sidewall of the tunnel has a distinct lining dislocation with a magnitude of 1.8 m.

Figure 6(a) shows the post-earthquake deformation distributed along the tunnel axis. The lining dislocation was concentrated within the 21 m zone, ranging from K1971 +390.4 to K1971+411.7, located near the interface between

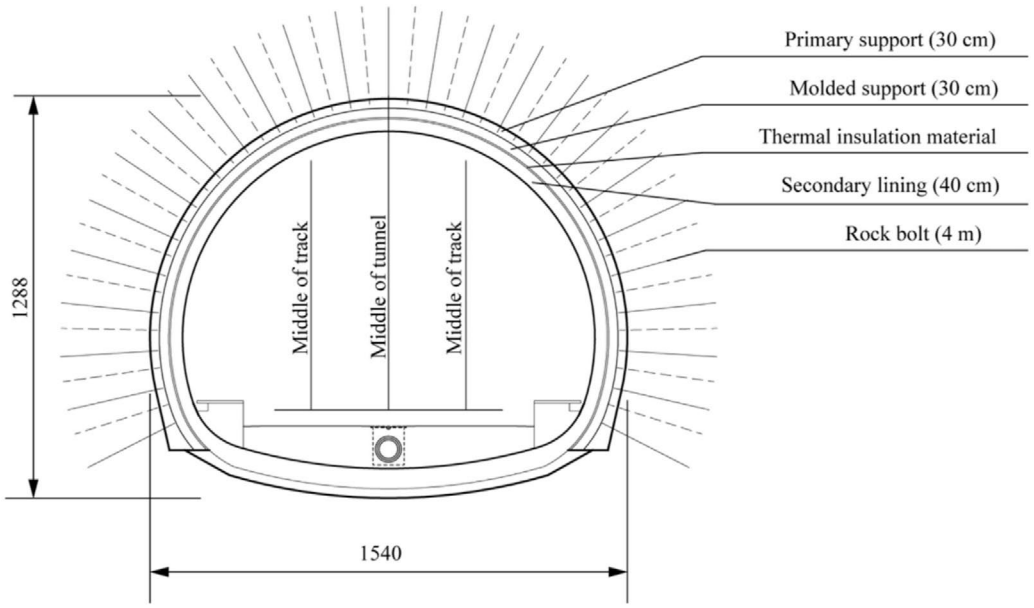

Fig. 4. Typical shape of tunnel structure. (Unit: cm)

Fig. 5. Dislocation and collapse of lining.

the fault and the hanging wall. The angle of intersection between the dislocation rupture and tunnel axis was about 50°. The lateral dislocation along the tunnel ranged from 1.5 to 2.0 m, and the longitudinal dislocation ranged from 0.3 to 0.8 m, due to the fault movement.

Figure 6(b) displays the deformation characteristics of different tunnel cross-sections along their length. It can be observed from the figure that tunnel sections close to the fault rupture plane exhibited an oval deformation due to the compression from surrounding rocks. In contrast, other sections far away from the rupture plane were only affected by the ground motion, and there was no obvious deformation.

3.1.2 Lining cracks

Lining cracks were distributed throughout the entire tunnel and exhibited different patterns in various zones. These cracks can be categorized into four main types: reticular cracks, inclined cracks, circumferential cracks, and longitudinal cracks, as shown in Fig. 7. Reticular and inclined cracks were the most concentrated crack patterns, which were mainly observed within the range from K1971+295 to K1971+695 close to the LLL Fault, where the lining suffered from compression and shear forces due to the fault dislocation effect. Circumferential cracks were the most widely distributed cracks along the tunnel lining, and most of these cracks were short and localized, primarily observed on the sidewalls and inverts of the tunnel. However, several circumferential cracks near the fault were notably longer, almost forming complete rings. These longer cracks were often accompanied by concrete lining spalling. Longitudinal cracks usually appeared on the track beds after track lifting, affected by the fault movement.

3.1.3 Lining spalling

The distribution of lining spalling was highly concentrated in specific sections of the Daliang Tunnel. Approximately 96% of the total lining spalling area occurred within a 996 m-long zone ranging from K1970+695 to K1971+691, as illustrated in Fig. 8. This zone was entirely located in the region of the IX-degree intensity and crossed the LLL Fault. Note that 295 m of that was situated within the fault zone, while 690 m was in the hanging wall and 11 m in the footwall. The remaining spalling was scattered over a large area extending more than 5 km along the tunnel, but occurred in much smaller quantities.

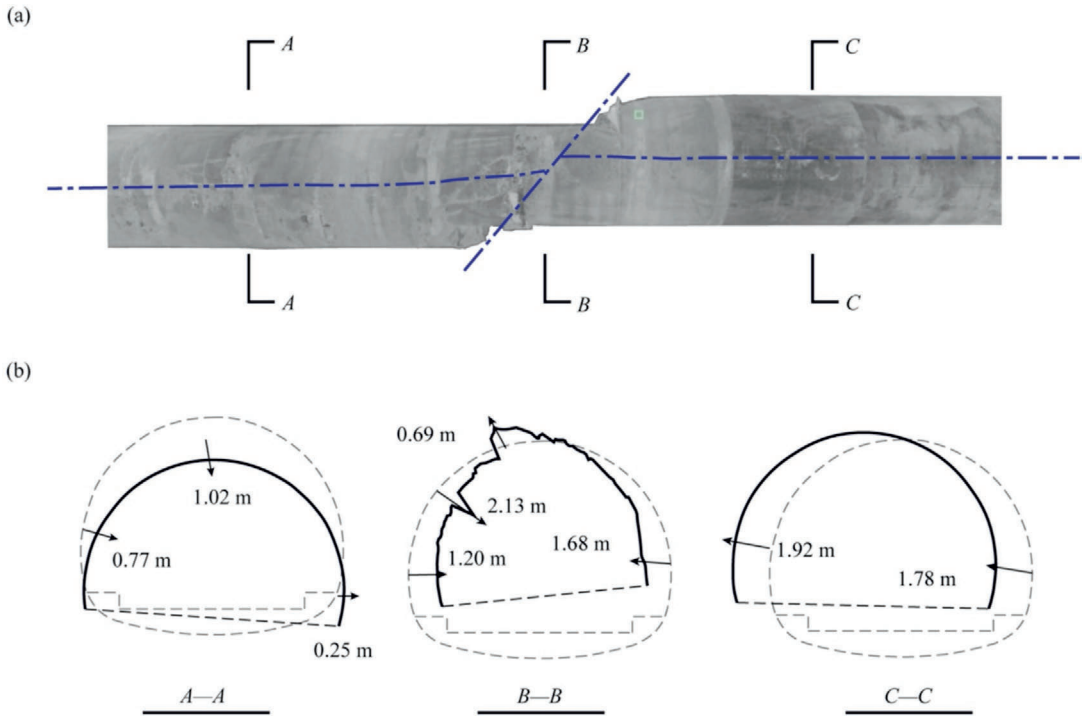

Fig. 6. Post-earthquake 3D laser scanning of (a) tunnel lining, and (b) deformed cross sections.

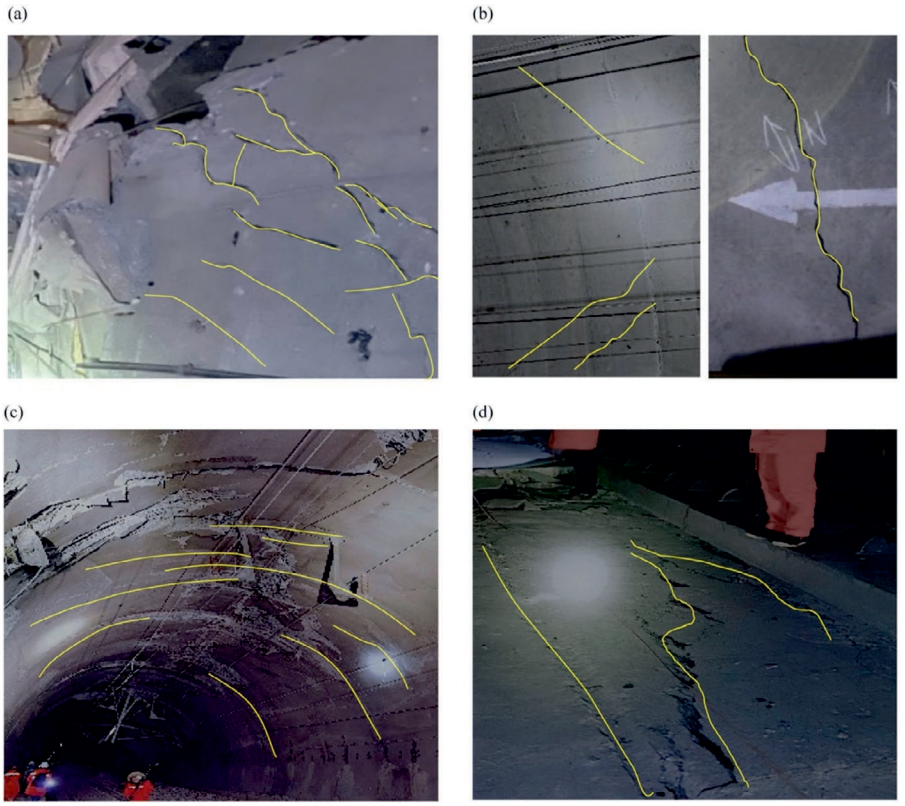

Fig. 7. Four types of cracks. (a) Reticular cracks, (b) inclined cracks, (c) circumferential cracks, and (d) longitudinal cracks.

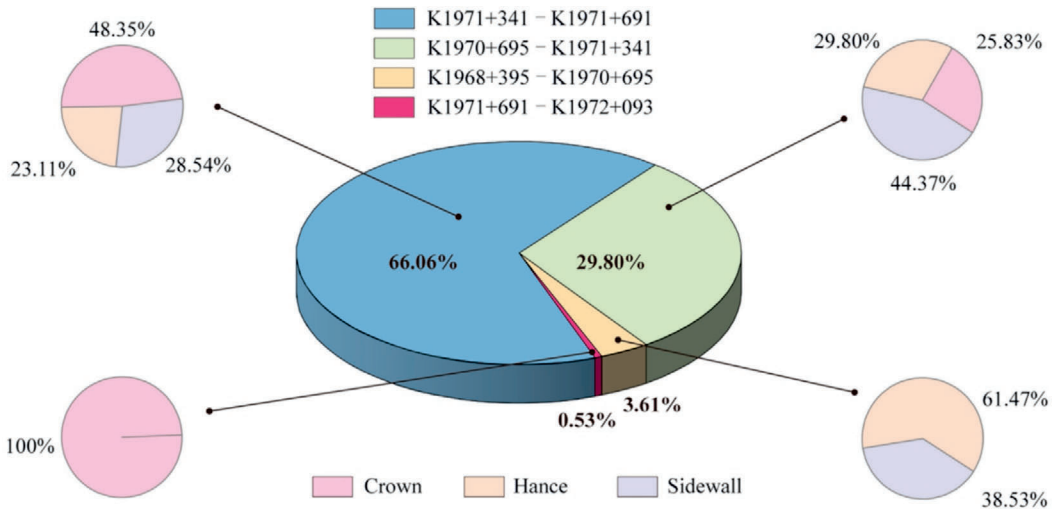

Fig. 8. Distribution of spalling. (Data from Zhang et al. (2022))

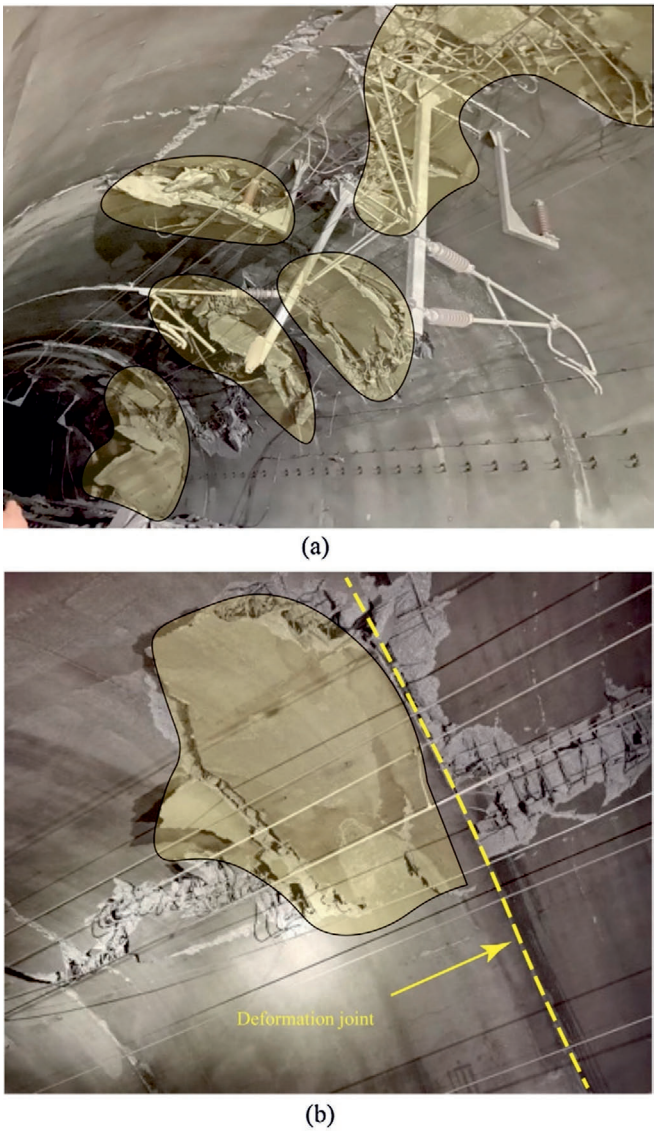

Fig. 9. Concrete spalling observed on (a) arches, and (b) along deformation joints.

Figure 8 also highlights the distribution of lining spalling at different tunnel sections along the tunnel. It can be seen from the figure that lining spalling was mainly observed on the tunnel crowns from K1970+695 to K1971+691, accounting for nearly 40% of the total spalling area, followed by the side walls with around 30%. In the range from K1970+695 to K1971+691, the lining spalling was continuous and extensive, often accompanied by reticular and inclined cracks (Fig. 9(a)). In other zones, the lining spalling was more sporadic, mainly concentrated around deformation joints (Fig. 9(b)).

3.1.4 Invert uplift

The invert uplift was mainly observed in a 350 m range in the vicinity of the LLL Fault, which led to significant damage to many non-structural members. Distribution of the invert uplift coincided with that of the lining dislocation, extending from K1971+341 to K1971+691.

In this region, invert filling materials were displaced and separated from the tunnel inverts reaching 20 cm. The track bed was uplifted into an A-shaped form, as illustrated in Fig. 10, with a maximum uplift of 0.7 m. The track slabs were tilted at an oblique angle of 40°. The concrete track bed broke into blocks, and the train tracks formed a wavy distortion. Additionally, the central drain gutter was sheared off, and its cover was lifted, resulting in flooding, as displayed in Fig. 11.

3.2 Damage assessment

The seismic damage to the Daliang Tunnel was assessed by the method introduced by Yu et al. (2016b). This method classifies damage severity into five levels based on both structural damage parameters and deformation: no damage (I), slight damage (II), moderate damage (III), severe damage (IV), and collapse (V). More details on the assessment criterion according to damage conditions of the tunnel structure are illustrated in Appendix A. The

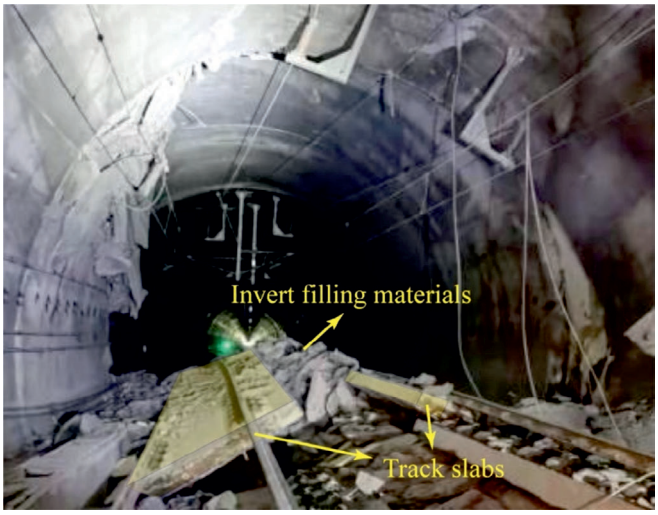

Fig. 10. Invert uplift.

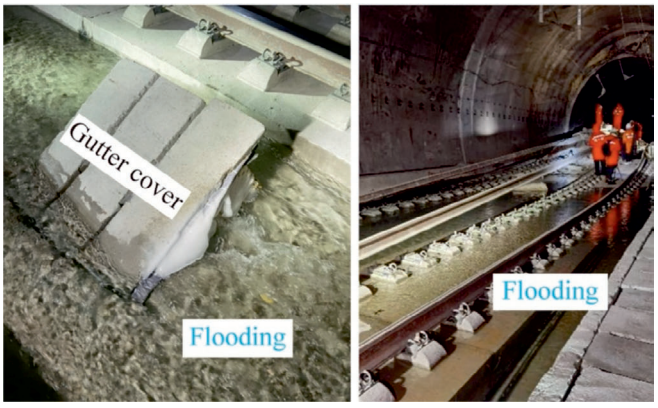

Fig. 11. Gutter cover uplift and flooding.

damage parameters include the length of cracks, area of spalling, dislocation of lining, and uplift of invert, while the tunnel deformation is determined by offset along the tunnel axis.

The distribution of assessment results and related parameters along the Daliang Tunnel is illustrated in Fig. 12. The most damaged sections, rated as collapse (V), spanned a total of 627 m, crossing the LLL Fault. Of this, 295 m lay entirely within the fault zone, with 197 m in the hanging wall and 135 m in the footwall. The tunnel sections assessed as severe damage (IV) were entirely located on the hanging wall and extended over 1250 m. Meanwhile, the rest of the 4673 m-long tunnel sections along the tunnel axis suffered from moderate (III) or only light damage (II).

It should be noted that the original design fortification intensity for the Daliang Tunnel was only VII-degree, much lower than the actual recorded earthquake intensity (IX-degree) during the Menyuan Earthquake. Even so, over 70% of the tunnel section did not suffer severe damage, demonstrating that the original design of the Daliang Tunnel provided considerable seismic performance. However, the tunnel section across the active fault experienced severe damage and completely collapsed, highlighting the lack of targeted design solutions for fault dislocations. It is worth noting that the hanging wall effect was also prominent, and thus, more concentrated and severe damage to the tunnel structure was observed in the hanging wall rather than the footwall.

The relationship between seismic damage of the tunnel lining and earthquake intensity is plotted in Fig. 12. It can be clearly observed from the figure that the tunnel section with a total length of 1880 m located in the VIII-degree intensity zone experienced only slight damage or remained intact, while the tunnel section situated in the IX-degree intensity zone was slightly to severely damaged and partially collapsed.

3.3 Damage zonation

It can be obtained from the seismic damage investigation of the Daliang Tunnel that the failure modes and deformation of the tunnel lining are distributed differently along the tunnel, which is correlated with geological conditions and seismic intensities of the region, as shown in Fig. 12. According to the geological conditions, the Daliang Tunnel can be divided into three distinct sections: the cross-fault section, the portal section, and the ordinary section, as explained in Table 1. The corresponding damage modes of these tunnel sections are also summarized in Fig. 13.

Clearly, the cross-fault section of the Daliang Tunnel suffered from the most severe damage, with the seismic damage to the entire section being evaluated as collapse (Fig. 13(b)). More specifically, the tunnel lining in this section experienced significant meter-level deformations, including lining dislocations and invert uplifts, along with non-structural failures such as electrical system breakdowns and flooding. Extensive and continuous concrete spalling was observed around the tunnel arch, and the cracks in the lining primarily appeared as reticular and inclined cracks, with some circumferential cracks also present.

Seismic damage patterns for the ordinary section of the tunnel are plotted in Fig. 13(c). Although the extent of damage varies due to differences in distance from the fault, the type of damage remains relatively consistent across this section. The observed damage for this tunnel section included concrete spalling, lining cracks, and leakage. Note that cracks in this section were primarily distributed in the circumferential and inclined forms, with a few longitudinal cracks. Comparatively, the portal sections of the Daliang Tunnel were less damaged. Both portal sections displayed a consistent damage mode characterized by localized spalling and circumferential cracks (Fig. 13(a) and (d)).

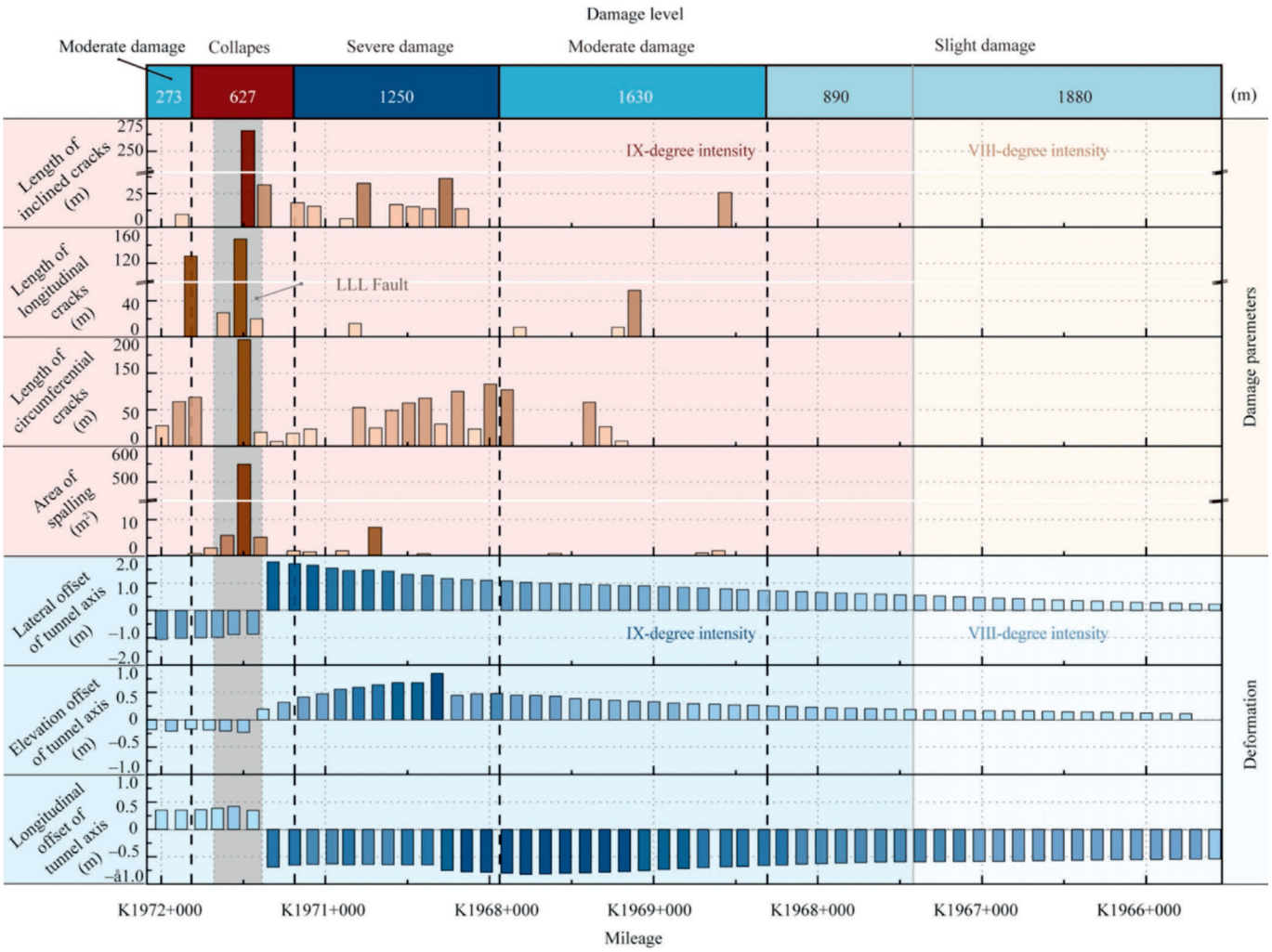

Fig. 12. Damage assessment and distribution of damage parameters and deformation. (Data from Zhang et al. (2022))

Table 1
Definition of different sections along the tunnel.

Zone	Mileage	Length (m)	Description
Cross-fault section	K1971+188–K1971+815	627	The cross-fault section is defined as the part of the tunnel that passes through the fault fracture zone and the surrounding parts affected by the fault movement.
Portal section	K1971+888–K1972+088; K1965+538–K1965+738	400	The portal section refers to the shallow buried parts of the tunnel portals and transition parts to the tunnel body.
Ordinary section	The remainder	5523	Except for the cross-fault section and the portal section, the remaining parts are named as the ordinary section.

4 Influence factors for seismic damage of cross-fault tunnels

The 2008 Wenchuan Earthquake was another devastating seismic event in China, with extensive and well-documented investigations. Numerous mountain tunnels located in the high earthquake intensity region with adverse geological conditions were damaged during this earthquake. Notably, these tunnels have been investigated by a number of researchers (Yu et al., 2016b), using the same evaluation standards for seismic damage of tunnel structures as described in Section 3.2 of this study. More importantly, both the 2008 Wenchuan Earthquake and the 2022 Menyuan Earthquake occurred in western China, and the regional geological conditions as well as the tunnel types are similar, which makes it valuable to compare the damage characteristics of tunnel structures during the

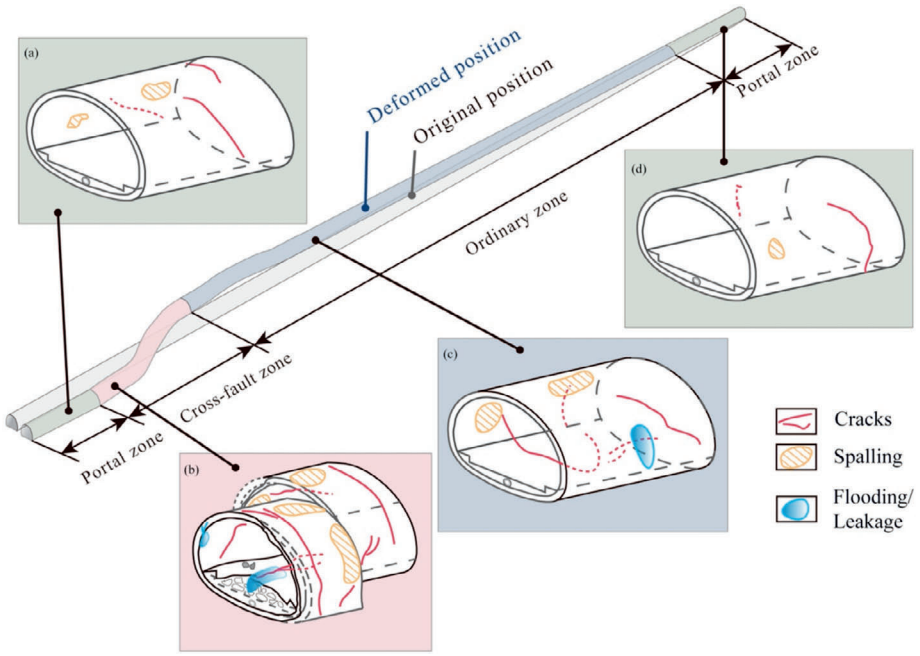

Fig. 13. Structural damage mode of each zone. (a) The northern portal zone, (b) cross-fault zone, (c) ordinary zone, and (d) the southern portal zone.

two earthquakes, so as to gain deeper insights into the damage mechanisms of cross-fault tunnels and their critical influencing factors.

According to the seismic investigation (Yu et al., 2016b), 55 tunnels were damaged during the Wenchuan Earthquake, while 2 tunnels were damaged in the Menyuan Earthquake. Note that all 57 tunnels were originally designed to withstand VII-degree seismic intensity. The detailed information and assessment data from both earthquakes have been compiled into a case database, as listed in Table B1 in Appendix B. This comparative analysis allows for a better understanding of the potential factors primarily affecting the seismic responses of cross-fault tunnels and provides additional evidence for developing more resilience-based design strategies, which will be discussed as follows.

4.1 Coupling effects of ground motion and fault dislocation

It can be obtained from the seismic damage investigation of the Daliang Tunnel that the seismic intensity and fault activity are the key factors affecting the tunnel damage severity. Note that these two factors have attracted significant attention from a number of researchers in historical case studies (Anastasopoulos et al., 2008; Kontogianni & Stiros, 2003). Figure 14 shows the relationship between tunnel damage characteristics and two factors, including seismic intensity and fault activity. It can be observed from the figure that tunnels crossing the same types of faults but located in higher seismic intensity regions were more likely to suffer severe damage. Tunnels

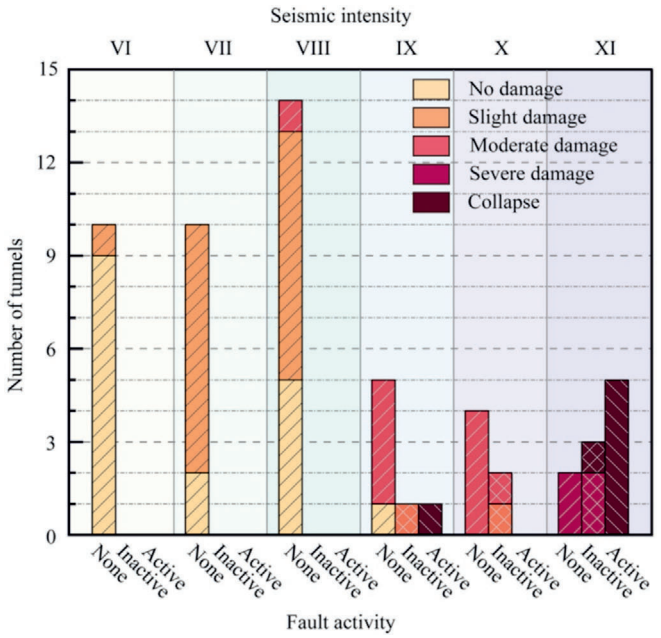

Fig. 14. Effects of the earthquake intensity and fault activity on tunnel damage level.

located in the VII and VIII-degree seismic intensity regions, but not crossing faults, experienced minor or no damage. However, tunnels situated in the regions with seismic intensity as high as X and XI degrees suffered more severe damage, even if there is no fault crossing, tunnel collapse would be expected. This indicates that it is important to provide the seismic intensity accurately for the design of tunnel

structures in seismic active areas, especially for the structural design under the action of strong ground motion.

It can also be observed from Fig. 14 that the fault activity would significantly exacerbate the seismic damage to tunnels. More specifically, tunnels located in areas with the same earthquake intensity but crossing faults consistently exhibited more severe damage than tunnels that did not cross faults. Besides, all the investigated tunnels crossing active faults in the XI-degree intensity zone have collapsed, which indicates that the coupling effect of strong ground motion and fault dislocation is prominent and should be considered in the seismic design for tunnel structures crossing the active fault.

Figure 14 indicates that 35 of the 57 investigated tunnels were located in VIII-degree intensity regions or higher, accounting for over 60% of the total. This suggests that the actual seismic loads during these two earthquakes exceeded the estimated design loads. This reveals the gap in current design methods, especially for sites with active faults, where seismic loads may be underestimated. Thus, understanding the coupling mechanism between ground motion and fault dislocation, as well as accurately estimating seismic loads, is essential for seismic design of cross-fault tunnels. The characterization of the geometric sizes and seismic histories of large fault zones can be very useful for estimating the possible maximum magnitude of earthquakes as well as predicting their recurrence behavior, which would be important for the assessment of caprock (or host rock) integrity over the long term.

4.2 Effects of deformation joints

Figure 15 illustrates the damage patterns of the cross-fault sections of the Longxi tunnel and the Daliang Tunnel, which were seriously damaged tunnels in the Wenchuan Earthquake and the Menyuan Earthquake, respectively. As can be seen from the figure, both the tunnel lining and surrounding rocks of the Longxi Tunnel across the fault completely collapsed, with invert uplift reaching 80 cm; while the cross-fault section of the Daliang Tunnel exhibited only lining collapse, accompanied by a significant 1.8 m lateral lining dislocation and 70 cm invert uplift.

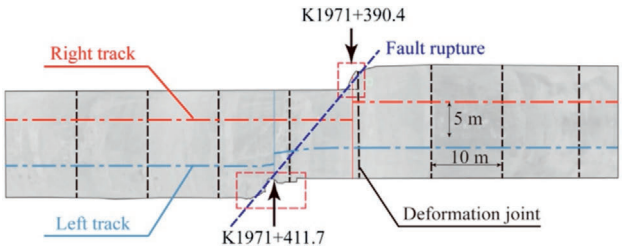

Fig. 16. Schematic diagram of the deformation pattern of the cross-fault zone along the Daliang Tunnel.

Surprisingly, the Daliang Tunnel did not suffer more severe structural failure, despite experiencing greater fault dislocation than the Longxi Tunnel. This anomalous observation can be attributed to the arrangement of deformation joints in the cross-fault section along the Daliang Tunnel.

Figure 16 shows the detailed arrangement of deformation joints along the cross-fault section of the Daliang Tunnel. It can be seen from the figure that the spacing for each adjacent deformation joint was set as 10 m. The intersection angle between the fault rupture and the tunnel axis was determined to be approximately 50°, based on the strike of the surface rupture. Because of this oblique intersection, the fault rupture may intersect on both sides of the tunnel near the joints, resulting in the lining dislocations observed around the deformation joints.

Note that these deformation joints act similarly to flexible joints, and their deformation mechanism has been addressed by a number of researchers and already validated by various experiments. Zhou et al. (2021) conducted a quasi-static experiment to analyze the deformation and failure mechanisms of tunnels with flexible joints subjected to strike-slip faults. Figure 17 compares experimental results with in-situ observations. Figure 17(a) and (b) illustrates experimental results for cross-fault tunnels without flexible joints, which correspond to the actual damage mode of the Longxi Tunnel (Fig. 17(c)). In contrast, Fig. 17(d) and (e) presents experimental results for cross-fault tunnels with flexible joints, compared to the damage observed in the Daliang Tunnel (Fig. 17(f)). The results

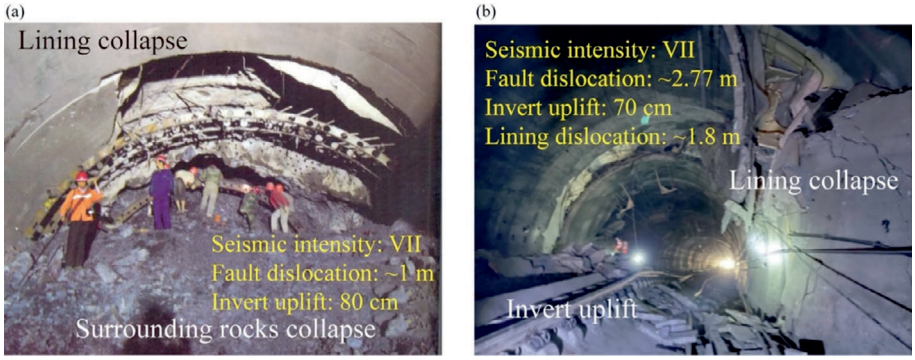

Fig. 15. Damage of the cross-fault zone in (a) Longxi Tunnel (Yu et al., 2016a), and (b) Daliang Tunnel.

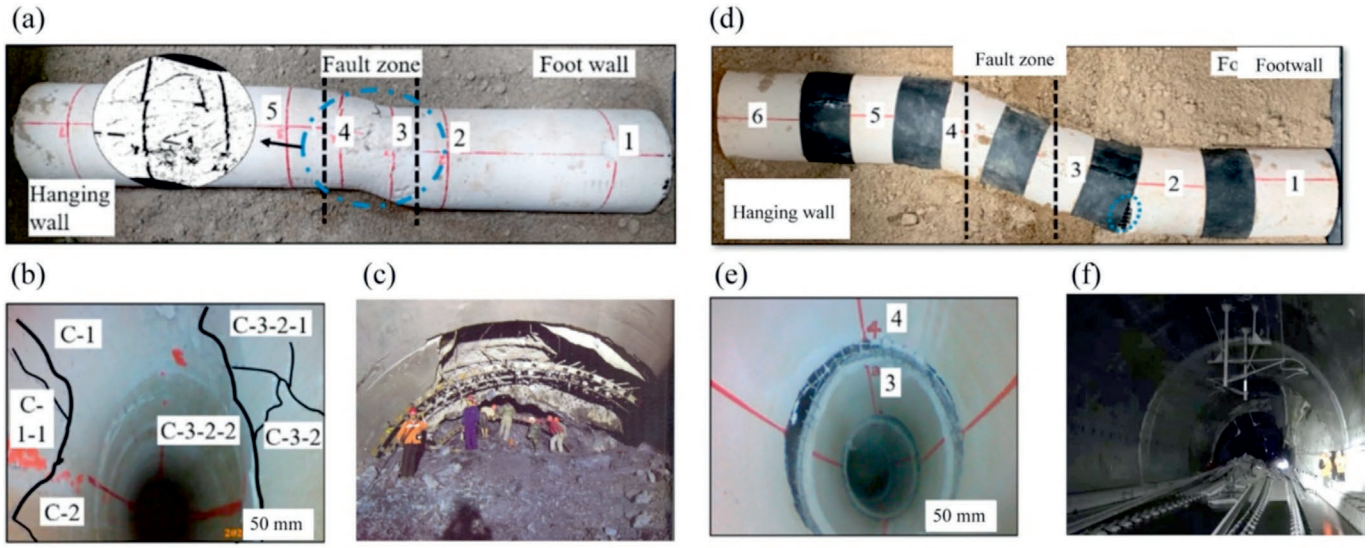

Fig. 17. Experimental results of deformation and cracking of the tunnel after fault dislocation with comparison of observed tunnel damage. (a) Experimental damage pattern of the tunnel without joints, (b) cross sectional damage patterns of lining without joints, (c) damage observed in the Longxi Tunnel, (d) experimental damage pattern of the tunnel with joints, (e) cross sectional damage patterns of lining without joints, and (f) damage observed in the Daliang Tunnel. (Yu et al., 2016a; Zhou et al., 2021)

shown in the figure are consistent with the damage observed in the Longxi Tunnel and the Daliang Tunnel, in which the tunnel with deformation joints exhibited less damage but greater deformation compared to the tunnel without joints. The observed structural damage and deformation were mainly concentrated around the flexible joints, suggesting that the deformation joints along the cross-fault section of the Daliang Tunnel play a protective role in mitigating widespread structural damage, while simultaneously leading to pronounced localized lining deformation near the fault rupture plane. This can be taken as an indicator that the deformation joints have dual characters: on one hand, they can effectively protect the main tunnel structure by adapting to the dislocation distribution along the cross-fault section of the tunnel during a seismic event; on the other hand, an added local deformation may be expected around the deformation joints, and furthermore the water proof capability of the joints should also be paid more attention in practical design.

4.3 Effects of the local topography

Fault dislocation is an important factor that causes severe damage to tunnels across active faults. Hence, it is essential to first assess the distribution of coseismic fault rupture dislocation under potential earthquake scenarios, carefully establish safety thresholds for different tunnel structures, and then carry out appropriate reinforcement measures for such fault-crossing infrastructure.

Figure 18 illustrates the distribution of coseismic surface rupture dislocation along the LLL Fault, which follows an approximate normal distribution consistent with the theoretical solution proposed by Okada (1985). The largest dislocation, approximately 3.7 m, occurred near the epicenter and gradually decreased on both sides. However, an abrupt increase in dislocation, around 2.8 m, was observed above the Daliang Tunnel, significantly larger than that at nearby observation points. Numerous studies on historical seismic events reveal that near-surface geological conditions and local topography are the primary factors contributing to such localized variability of fault dislocation (Guo et al., 2019; Langer et al., 2019; Li & Barnhart, 2020; Milliner et al., 2015; Reitman et al., 2022).

Combined with the field investigation near the Daliang Tunnel, it can be concluded that the slope instability may be one of the potential causes for this localized amplification of fault rupture dislocation. Figure 19 shows several landslides distributed along the main surface rupture zone of the earthquake, one of which is located directly on the slope above the Daliang Tunnel. Note that the near-surface soils in this area are loose and unstable, especially near the northern portal of the Daliang Tunnel, with a slope gradient of more than 30%, which can be regarded as a steep slope. As a result, landslides and slope instability are more likely to occur along these major surface ruptures.

The impact of local topography on rupture propagation and surface dislocation has gained increased attention. Shi et al. (2020) conducted a series of 1*g* physical model tests and reproduced the rupture propagation in the local site with inclined ground surfaces. Their experimental results indicate that, compared with flat ground conditions, inclined ground surfaces tend to develop a wider fault rupture zone accompanied by significantly larger surface dislocation. More importantly, the presence of inclined topography induces anisotropic initial stress conditions in the near-surface soil mass. Under the combined effects of

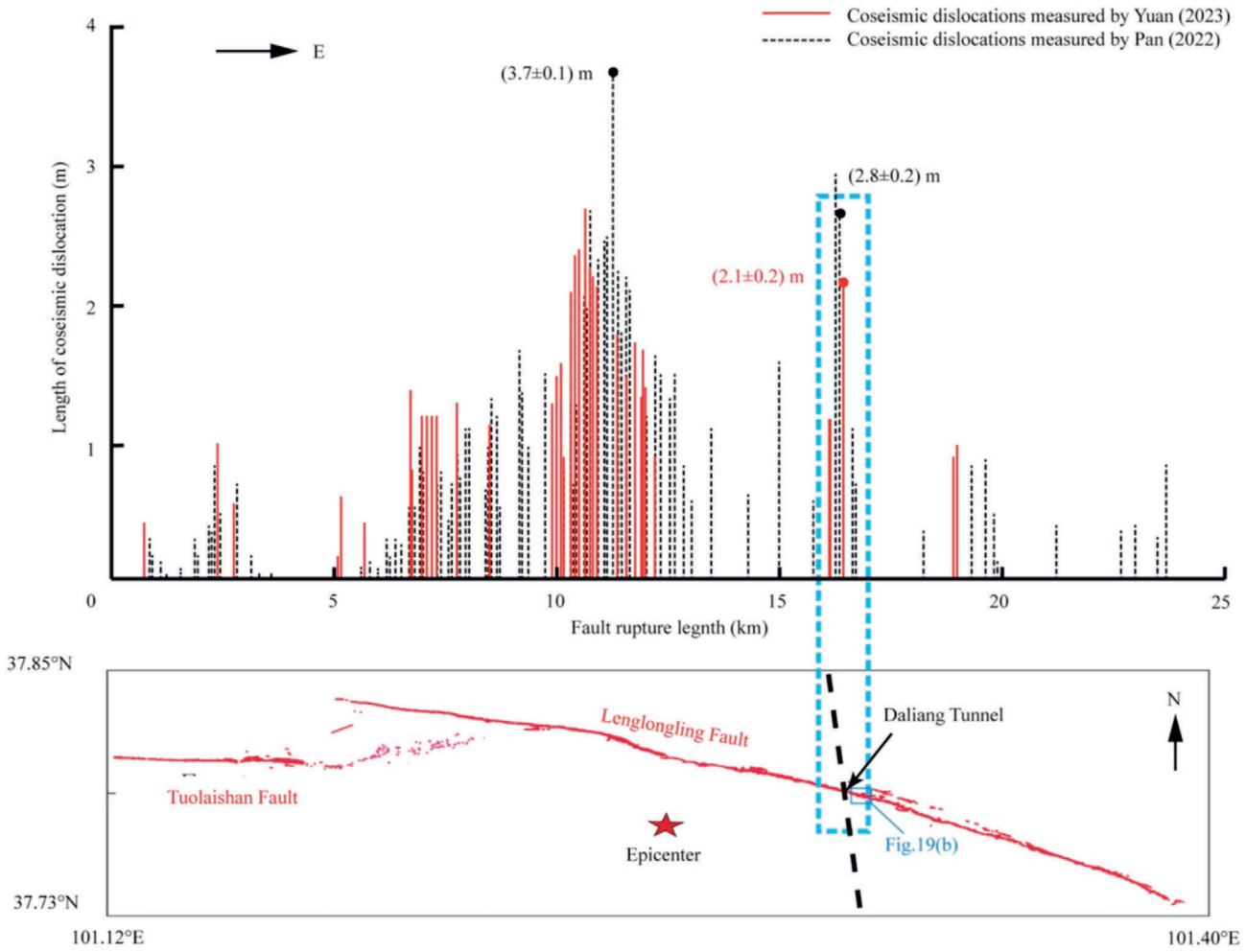

Fig. 18. Horizontal coseismic dislocations along the surface rupture zone of the 2022 Menyuan Earthquake. (Modified from Pan et al. (2022) and Yuan et al. (2023))

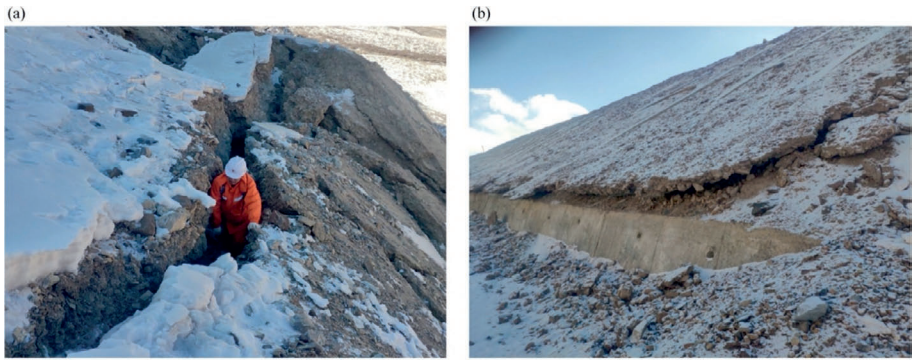

Fig. 19. Slide of slopes along the primary rupture of the LLL Fault. (a) Slope slide observed along the LLL Fault, and (b) slope instability near the Daliang Tunnel site.

fault rupture propagation and gravitational loading, additional mechanical disturbances may trigger local slope instability, leading to the formation of secondary strain concentration zones. With continued rupture evolution, these secondary zones can gradually interact with and eventually connect to the primary fault rupture path, resulting in a more complex and intensified surface rupture pattern.

These observations provide a plausible explanation for the pronounced fault dislocation and severe lining damage observed at the Daliang Tunnel site. The local topographic relief and site-specific geotechnical conditions are strongly

correlated with the spatial variability of fault dislocation, which may indirectly contribute to the meter-scale lining offset recorded in the tunnel. In addition, factors such as focal depth and fault plane properties are also expected to influence the heterogeneity of fault dislocation. Therefore, further investigation into the intrinsic mechanisms governing fault dislocation variability is essential, as it can provide a scientific basis for tunnel route selection and seismic resilience design of cross-fault tunnels.

5 Suggestions for seismic resilience design of cross-fault tunnels

5.1 Requirements of seismic resilience design

The collapse of the cross-fault section of the Daliang Tunnel resulted in a cessation of railway operations for over ten months, leading to substantial economic losses. This highlights the importance of maintaining operational stability as well as ensuring structural safety. Hence, it is suggested that more attention should be paid to the seismic performance of cross-fault tunnels, and the resilience-based design principles should be provided for tunnels in seismically active areas.

Seismic resilience design for tunnels can be categorized into three stages: (a) the tunnel should remain in good condition throughout its life cycle; (b) under strong seismic activity or fault dislocation, the tunnel should preserve structural and system stability, ensuring safety and minimal disruption; and (c) in the event of destructive damage, the tunnel should be able to quickly return to its original state through self-repair or external intervention, enabling swift restoration of operations.

5.2 Strategies for seismic resilience design

5.2.1 Formulated strategies for different tunnel sections

Most mountain tunnels span kilometers and traverse various geological strata, each with distinct lithology and seismic intensity, resulting in diverse tunnel sections that exhibit different failure modes. For example, the Daliang Tunnel experienced varying degrees of damage along its length, with distinct failure modes in each tunnel section (cross-fault section, tunnel portal section, and ordinary section), as discussed in Section 3.3. Therefore, seismic fortification measures should be formulated according to the specific characteristics of each tunnel section subjected to ground motions and fault dislocation, which can be classified into two parts:

(1) Site zonation: The proposed strategy begins with a comprehensive site zonation process that systematically assesses seismic hazards through the identification and characterization of active faults with potential engineering hazards. This involves applying statistical modeling theory to establish the distribution patterns of dislocations and deformations in both surface and near-surface regions, while probabilistic analysis methods are employed to predict potential fault dislocations under various exceedance probabilities. The assessment further incorporates near-field vibration characteristics, including ground vibration amplitude, velocity impulse period, pulse onset timing, and vertical component percentage. By integrating active fault deformation field characteristics with near-field strong ground vibration parameters, a comprehensive seismic hazard assessment is conducted, leading to the development of site defense zonation maps with quantified design loading levels.
(2) Structural segmentation: The structural segmentation approach complements the site zonation by analyzing seismic damage distribution patterns along tunnel structures crossing active fault zones, particularly focusing on the relationship between damage severity and distance from the fault. This analysis informs the establishment of seismic defense levels based on the tunnel's engineering importance classification. The integration of site zonation results with seismic defense levels enables the definition of specific performance objectives for tunnel structures under different seismic scenarios. This comprehensive approach culminates in the development of guidelines for segmental seismic defense of tunnels crossing active fault zones, specifying mitigation measures and performance requirements, thereby forming a theoretical framework for zonation-based and segmental seismic defense strategies in seismically active regions.

5.2.2 Multi-stage resilience design framework

Based on the aforementioned seismic damage investigation on tunnels across the fault, the need for rapid recovery of tunnel operations under extreme hazard conditions has led to the development of a seismic resilience design framework for cross-fault tunnels, which can be classified into three stages:

(1) Resisting/mitigating: For frequent-level seismic hazards with minor ground motion and no fault dislocation, strategies such as rock reinforcement and shock absorption layers should be adopted to improve the seismic capacity of tunnel structures and reduce the seismic energy transfer to the structure, and thereby minimize the structural damage.
(2) Adapting: For moderate-level seismic hazards, such as strong ground motion or minor fault dislocation, self-adaptive design measures, including flexible

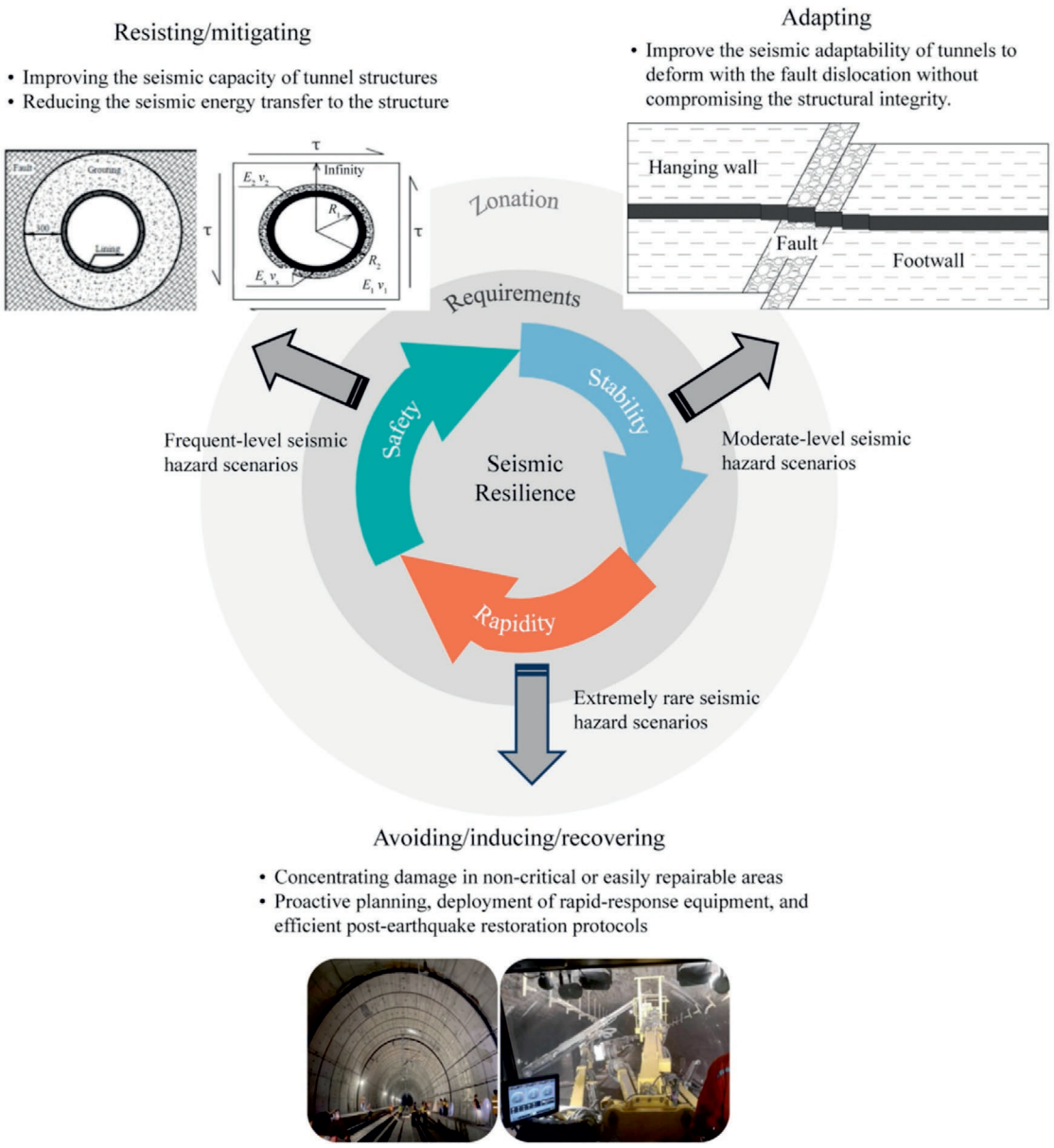

Fig. 20. Framework of the seismic resilience design strategies for cross-fault tunnels.

joints along the tunnel, should be used to improve the seismic adaptability of tunnels to deform with the fault dislocation without compromising the structural integrity. These flexible joints could help the tunnel adapt to the deformation caused by fault dislocation and surrounding rock movement.

(3) Avoiding/inducing/recovering: For extremely rare seismic hazards, such as the coupling effects of strong ground motions and large fault dislocations, a "cut-loss strategy" should be prioritized. This involves employing innovative structural systems or advanced materials designed to concentrate damage in non-critical or easily repairable areas, thereby safeguarding the main structure. To further enhance the seismic resilience of tunnels crossing active faults, protective measures should be systematically implemented. These include proactive planning, deployment of rapid-response equipment, and efficient post-earthquake restoration protocols.

This comprehensive three-stage resilience design strategy, that is resisting/mitigating, adapting, and avoiding/inducing/recovering, could provide a resilience framework for improving the seismic resilience of cross-fault tunnels,

ensuring both the structural safety and operational stability of tunnels across faults during and after seismic events (see Fig. 20).

6 Conclusions

The Daliang Tunnel suffered from minor to heavy damage under the 2022 Menyuan Earthquake with a moment magnitude of 6.6. The damage was mainly observed at the tunnel section crossing the LLL Fault, where the cross-fault section completely collapsed due to the large fault dislocation. The structural damage of the tunnel can be classified into four types: lining dislocation, lining cracks, spalling, and invert uplift. The severity of damage to the tunnel is strongly correlated with the distance to the fault, as well as the seismic intensity, which emphasizes the need for special design of the cross-fault tunnel section. The failure modes of the tunnel lining are distributed differently for each tunnel section (cross-fault section, tunnel portal section, and ordinary section) along the tunnel length. Comparatively, the cross-fault section of the tunnel experienced the most severe damage, including large-scale lining dislocations and invert uplift, whereas the ordinary and portal sections of the tunnel suffered mostly minor damage such as spalling and localized cracks.

This study synthesizes the key factors governing the seismic damage of cross-fault tunnels, encompassing seismic loading conditions, structural configurations, and fault dislocation characteristics, based on post-earthquake evidence from the Daliang Tunnel damaged during the 2022 Menyuan Earthquake and comparable tunnel failures observed in the 2008 Wenchuan Earthquake. Seismic damage investigation indicates that the coupling effect of strong ground motion and fault dislocation is the main cause for structural damage and should be considered in the seismic design for tunnel structures crossing the active fault. The deformation joint system adopted in the cross-fault tunnels is effective in mitigating large-scale structural damage. However, this protective effect is accompanied by significant localized lining deformation in the vicinity of the fault rupture plane, highlighting an inherent trade-off in cross-fault tunnel seismic design. The local variability of fault rupture dislocation may also have adverse effects on tunnel collapse; for instance, the instability of the overlying slope may have contributed to the local amplification of the fault dislocation along the Daliang Tunnel, as observed from the seismic investigation.

Furthermore, seismic resilience objectives for cross-fault tunnels are identified, and corresponding design-oriented measures are summarized to enhance the overall seismic performance and damage tolerance of tunnels intersecting active faults. It is suggested that multi-stage formulated strategies should be provided for different tunnel sections based on the damage observation and zonation of the investigated tunnels. Accordingly, a three-stage resilience design framework, including resisting/mitigating, adapting, and avoiding/inducing/recovering stages, is proposed to ensure both the structural safety and operational stability for cross-fault tunnels under seismic events.

These findings and recommendations in this paper are intended to inform future research and contribute to the development of improved seismic design strategies for cross-fault tunnels. Additional studies are needed on the coupling mechanisms between ground motions and fault dislocations, the spatial variability of fault dislocation distribution, and the development of new seismic resilient structural systems. It is expected that the results will be the focus of future publications.

Data availability

The data that support the findings of this study are available from the corresponding author upon reasonable request.

CRediT authorship contribution statement

Haitao Yu: Writing – review & editing, Supervision, Funding acquisition, Writing – original draft, Investigation, Conceptualization. **Yibo Wei:** Data curation, Writing – original draft, Investigation, Conceptualization. **Yong Yuan:** Writing – review & editing, Investigation, Supervision. **Guoliang Li:** Writing – review & editing, Data curation, Investigation. **Hehua Zhu:** Funding acquisition, Supervision, Writing – review & editing.

Declaration of competing interest

Dr. Hehua Zhu is an editor-in-chief for *Underground* Space and was not involved in the editorial review or the decision to publish this article. All authors declare that there are no competing interests.

Acknowledgement

The research was supported by the Natural Science Foundation of China (Grant Nos. 42177134 and 42477141), the Natural Science Foundation of Qinghai Province (Grant No. 2024-ZJ-717), and the Fundamental Research Funds for the Central Universities of China.

Appendix A

Table A1
Damage level classification for mountain tunnels. (Modified from Yu et al. (2016b))

Tunnel classification	Damage level	Damage description
I	No damage	No damage detectable by visual inspection. Perfect functionality.
II	Slight damage	Slight damage, small cracking (width < 3 mm, length < 5 cm) in the lining and construction joints. Localized deterioration and surface spalling. No effect on traffic.
III	Moderate damage	Regional small-scale cracking (3 mm < width < 30 mm, 5 m < length < 10 m), small spalling, and reinforcing steel bar exposed (area < 1 m^2). Effect on traffic. Compromised functionality
IV	Severe damage	A large number of cracks (width > 30 mm, length > 10 m), spalling and reinforcing steel bar exposed (1 m^2 < area < 3 m^2), shear off of lining (relative displacement > 20 cm), uplift or differential movement of tunnel pavement and invert (height > 20 cm). Traffic service interruption.
V	Collapse	A large number of cracks, large-scale spalling (area > 3 m^2), and reinforcing steel bar exposed and distorted, shear off of lining, pavement cracking, and invert uplift or collapse.

Appendix B

Table B1
Summary of the tunnel information and damage assessment (Chen, 2012; Shen et al., 2014; Wang et al., 2009; Yu et al., 2016b).

Tunnel name	Fortification intensity	Earthquake intensity	Fault activity	Damage level	Earthquake
Longxi	VII	XI	Active	V	Wenchuan
Jiujiaya	VII	XI	Active	V	Wenchuan
Youyi	VII	XI	Active	V	Wenchuan
Baiyunding	VII	XI	Active	V	Wenchuan
Longdongzi	VII	XI	Active	V	Wenchuan
Zipingpu	VII	XI	Inactive	V	Wenchuan
Daliang	VII	IX	Active	V	Menyuan
Shaohuoping	VII	XI	Inactive	IV	Wenchuan
Longchi	VII	XI	Inactive	IV	Wenchuan
Niujiaya	VII	XI	None	IV	Wenchuan
Zaojiaowan	VII	XI	None	IV	Wenchuan
Maanshi	VII	X	Inactive	III	Wenchuan
Maojiawan	VII	X	None	III	Wenchuan
Panlongshan	VII	X	None	III	Wenchuan
Futang	VII	X	None	III	Wenchuan
Futangba	VII	X	None	III	Wenchuan
Gengda	VII	IX	None	III	Wenchuan
Chediguan	VII	IX	None	III	Wenchuan
Taoguan	VII	IX	None	III	Wenchuan
Caopo	VII	IX	None	III	Wenchuan
Sanpanzi	VII	VIII	None	III	Wenchuan
Dankanliangzi	VII	X	Inactive	II	Wenchuan
Yinxing	VII	VIII	None	II	Wenchuan
Huayanzi	VII	VIII	None	II	Wenchuan
Chenjiashan#1	VII	VIII	None	II	Wenchuan
Chenjiashan#2	VII	VIII	None	II	Wenchuan
Fenshuiling	VII	VIII	None	II	Wenchuan
Qiujiapo	VII	VIII	None	II	Wenchuan
Mingyuexia	VII	VIII	None	II	Wenchuan
Feixianguan	VII	VIII	None	II	Wenchuan
Qujiapo	VII	VII	None	II	Wenchuan
Mafu	VII	VII	None	II	Wenchuan
Tianjiaba	VII	VII	None	II	Wenchuan
Caomigang	VII	VII	None	II	Wenchuan
Hongfu	VII	VII	None	II	Wenchuan
Wangong	VII	VII	None	II	Wenchuan
Shunhe	VII	VII	None	II	Wenchuan
Banyang	VII	VII	None	II	Wenchuan
Shiziping	VII	VI	None	II	Wenchuan
Qilianshan	VII	IX	None	II	Menyuan

(*continued on next page*)

Table B1 (*continued*)

Tunnel name	Fortification intensity	Earthquake intensity	Fault activity	Damage level	Earthquake
Qinglinpo	VII	VIII	None	I	Wenchuan
Shiwengzi	VII	VIII	None	I	Wenchuan
Guanyazi	VII	VIII	None	I	Wenchuan
Xinjiagou	VII	VIII	None	I	Wenchuan
Qipanguan	VII	VIII	None	I	Wenchuan
Feishaguan	VII	VII	None	I	Wenchuan
Shitigou	VII	VII	None	I	Wenchuan
Xiaoqiudi	VII	VI	None	I	Wenchuan
Jiujiapeng	VII	VI	None	I	Wenchuan
Zagunao	VII	VI	None	I	Wenchuan
Luobugang	VII	VI	None	I	Wenchuan
Zhegushan	VII	VI	None	I	Wenchuan
Shizikou	VII	VI	None	I	Wenchuan
Xuequ#1	VII	VI	None	I	Wenchuan
Xuequ#2	VII	VI	None	I	Wenchuan
Baixionggou	VII	VI	None	I	Wenchuan
Xiquanyan	VII	IX	None	I	Wenchuan

References

Anastasopoulos, I., Gerolymos, N., Drosos, V., Georgarakos, T., Kourkoulis, R., & Gazetas, G. (2008). Behaviour of deep immersed tunnel under combined normal fault rupture deformation and subsequent seismic shaking. *Bulletin of Earthquake Engineering, 6*(2), 213–239.

Ansari, A., El-Hussain, I., Deif, A., Mohamed, A. M. E., Al-Shijbi, Y., Al-Jabri, K., et al. (2024). Seismic vulnerability assessment and fragility analysis of tunnels in Oman: Development of risk matrices and functionality guidelines. *Structures, 69*, 107428.

Asakura, T., & Sato, Y. (1996). Damage to mountain tunnels in hazard area. *Soils and Foundations, 36*, 301–310.

Asakura, T. (1997). Mountain tunnels performance in the 1995 Hyogo-ken-Nanbu earthquake. In *The 2nd international symposium on recent advances in exploration geophysics (RAEG 1997)* (pp. cp-422). European Association of Geoscientists & Engineers.

Chen, L. (2012). *Seismic investigation on highways in the Wenchuan Earthquake: Report on highways' damage in the Wenchuan Earthquake* (1st ed.). China Communications Press (in Chinese).

China Earthquake Administration. (2022). Qinghai Menyuan Magnitude 6.9 Earthquake Intensity Map. (2022-01-11). Retrieved from https://www.cea.gov.cn/cea/xwzx/fzjzyw/5646200/index.html (in Chinese).

China Railway Eryuan Engineering Group Co., Ltd. (2016). *TB 10003—2016:* Code for Design of Railway Tunnel. China Railway Press, Beijing (in Chinese).

Guo, P., Han, Z. J., Ran, H. L., Luo, J. H., Wu, G., & Yuan, R. M. (2019). Co-seismic surface rupture of Papatea fault and reactivation mechanism of the Clarence landslide during the 2016 Mw7. 8 Kaikoura earthquake, New Zealand. *Bulletin of Engineering Geology and the Environment, 78*(5), 3055–3068.

Kontogianni, V. A., & Stiros, S. C. (2003). Earthquakes and seismic faulting: Effects on tunnels. *Turkish Journal of Earth Sciences, 12*(1), 153–156.

Langer, L., Gharti, H. N., & Tromp, J. (2019). Impact of topography and three-dimensional heterogeneity on coseismic deformation. *Geophysical Journal International, 217*(2), 866–878.

Li, S., & Barnhart, W. D. (2020). Impacts of topographic relief and crustal heterogeneity on coseismic deformation and inversions for fault geometry and slip: A case study of the 2015 Gorkha earthquake in the Central Himalayan Arc. *Geochemistry, Geophysics, Geosystems, 21* (12), e2020GC009413.

Liang, K., He, Z. T., Jiang, W. L., Li, Y. S., & Liu, Z. M. (2022). Surface rupture characteristics of the Menyuan Ms 6.9 earthquake on January 8, 2022, Qinghai Province. *Seismology and Geology, 44*(1), 256–278 (in Chinese).

Milliner, C. W., Dolan, J. F., Hollingsworth, J., Leprince, S., Ayoub, F., & Sammis, C. G. (2015). Quantifying near-field and off-fault deformation patterns of the 1992 Mw 7.3 Landers earthquake. *Geochemistry, Geophysics, Geosystems, 16*(5), 1577–1598.

Ministry of Housing and Urban-Rural Development of the People's Republic of China. (2010). *GB 50010—2010: Code for Design of Concrete Structures*. China Architecture & Building Press, Beijing (in Chinese).

Okada, Y. (1985). Surface deformation due to shear and tensile faults in a half-space. *Bulletin of the Seismological Society of America, 75*(4), 1135–1154.

Pan, J., Li, H., Chevalier, M., Liu, D., Li, C., Liu, F., Wu, Q., Lu, H., & Jiao, L. (2022). Coseismic surface rupture and seismogenic structure of the 2022 M.6.9 Menyuan earthquake. *Qinghai Province. Acta Geologica Sinica, 96*, 215–231 (in Chinese).

Reitman, N. G., Mueller, K. J., & Tucker, G. E. (2022). Surface slip variability on strike-slip faults. *Earth Surface Processes and Landforms, 47*(4), 908–935.

Shen, Y. S., Wang, Z. Z., Yu, J., Zhang, X., & Gao, B. (2020). Shaking table test on flexible joints of mountain tunnels passing through normal fault. *Tunnelling and Underground Space Technology, 98*, 103299.

Shen, Y., Gao, B., Yang, X., & Tao, S. (2014). Seismic damage mechanism and dynamic deformation characteristic analysis of mountain tunnel after Wenchuan earthquake. *Engineering Geology, 180*, 85–98.

Shi, J. S., Ling, D. S., Hu, C. B., & Tu, F. B. (2020). Study on reverse fault rupture propagation through sand with inclined ground surface. *Engineering Geology, 276*, 105768.

Wang, W. L., Wang, T. T., Su, J. J., Lin, C. H., Seng, C. R., & Huang, T. H. (2001). Assessment of damage in mountain tunnels due to the Taiwan Chi-Chi Earthquake. *Tunnelling and Underground Space Technology, 16*(3), 133–150.

Wang, Z., Gao, B., Jiang, Y., & Yuan, S. (2009). Investigation and assessment on mountain tunnels and geotechnical damage after the Wenchuan earthquake. *Science in China Series E: Technological Sciences, 52*(2), 546–558.

Wang, Z. Z., & Zhang, Z. J. S. D. (2013). Seismic damage classification and risk assessment of mountain tunnels with a validation for the 2008 Wenchuan earthquake. *Soil Dynamics and Earthquake Engineering, 45*, 45–55.

Yu, H., Chen, J., Bobet, A., & Yuan, Y. (2016a). Damage observation and assessment of the Longxi tunnel during the Wenchuan earthquake. *Tunnelling and Underground Space Technology, 54*, 102–116.

Yu, H. T., Chen, J. T., Yuan, Y., & Zhao, X. (2016b). Seismic damage of mountain tunnels during the 5.12 Wenchuan earthquake. *Journal of Mountain Science, 13*(11), 1958–1972.

Yuan, D., Xie, H., Su, R., Li, Z., Wen, Y., Si, G., Xue, S., Chen, G., Liu, B., Liang, S., Peng, H., Duan, L., & Wei, S. (2023). Characteristics of co-seismic surface rupture zone of Menyuan Ms6.9 earthquake in Qinghai Province on January 8, 2022 and seismogenic mechanism. *Chinese Journal of Geophysics, 66*(1), 229–244 (in Chinese).

Zhang, L.F., Li, R.H., Liu, H., Fang, Z.B., Wang, H.B., & Yu, H.T. (2020). A review on seismic response and aseismic measures of fault-crossing tunnels, In *IOP Conference Series: Earth and Environmental Science*, *570*, Article 052046.

Zhang, W., Li, M., Ji, Y. P., Li, G. L., Zhao, L. X., & Li, S. G. (2022). Analysis and enlightenment of typical failure characteristics of tunnels caused by the Menyuan M6.9 earthquake in Qinghai Province. *China Earthquake Engineering Journal, 44*, 661–669 (in Chinese).

Zhang, X., Jiang, Y., Hirakawa, Y., Cai, Y., & Sugimoto, S. (2019). Correlation between seismic damages of Tawarayama tunnel and ground deformation under the 2016 Kumamoto earthquake. *Rock Mechanics and Rock Engineering, 52*(7), 2401–2413.

Zhang, X., Jiang, Y., & Sugimoto, S. (2018). Seismic damage assessment of mountain tunnel: A case study on the Tawarayama tunnel due to the 2016 Kumamoto Earthquake. *Tunnelling and Underground Space Technology, 71*, 138–148.

Zhao, X., Li, R., Yuan, Y., Yu, H., Zhao, M., & Huang, J. (2022). Shaking table tests on fault-crossing tunnels and aseismic effect of grouting. *Tunnelling and Underground Space Technology, 125*, 104511.

Zhou, G., Sheng, Q., Cui, Z., Wang, T., & Ma, Y. (2021). Investigating the deformation and failure mechanism of a submarine tunnel with flexible joints subjected to strike-slip faults. *Journal of Marine Science and Engineering, 9*(12), 1412.